A constitutive hemorheological model addressing both the deformability and aggregation of red blood cells

Cite as: Phys. Fluids **32**, 103103 (2020); https://doi.org/10.1063/5.0022493
Submitted: 21 July 2020 . Accepted: 09 September 2020 . Published Online: 05 October 2020

Pavlos S. Stephanou

Physics of Fluids ARTICLE scitation.org/journal/phf

A constitutive hemorheological model addressing both the deformability and aggregation of red blood cells

Cite as: Phys. Fluids 32, 103103 (2020); doi: 10.1063/5.0022493
Submitted: 21 July 2020 • Accepted: 9 September 2020 •
Published Online: 5 October 2020

Pavlos S. Stephanou[a)]

AFFILIATIONS

Department of Chemical Engineering, Cyprus University of Technology, P.O. Box 50329, 3603 Limassol, Cyprus

[a)]**Author to whom correspondence should be addressed:** pavlos.stefanou@cut.ac.cy. **Tel.:** +357-25-002394. **Fax:** +357-25-002668

ABSTRACT

Red blood cells (RBCs) in physiological conditions are capable of deforming and aggregating. However, both deformation and aggregation are seldom considered together when modeling the rheological behavior of blood. This is particularly important since each mechanism is dominant under specific conditions. To address this void, we herein propose a new model that accounts for the deformability of red blood cells, by modeling them as deformed droplets with a constant volume, and of their aggregation, by properly characterizing the network formed by red blood cells under small shear rates. To derive the model, we employ non-equilibrium thermodynamics that allows us to consistently couple the two mechanisms and guarantees model admissibility with the thermodynamic laws. Relative to our previous model, which addresses the rheological behavior of non-aggregating deformable red blood cells, one additional structural variable, λ, to properly characterize the network formed by RBCs, and another additional parameter, ε, that quantifies the relative importance between the regeneration/buildup and flow-induced breakup of the network, are considered here. The new model predicts a yield shear stress, in accord with experimental data, but also predicts non-vanishing yield normal stresses. Although no rheological measurements of yield normal stresses of blood have been reported in the literature, the recent measurement of yield normal stresses of other yield stress fluids indicates their potential existence in blood as well. We show that the new model is in complete accord with the experimental rheological behavior of normal blood in both steady-state and transient (step-change in shear-rate) simple shear.

I. INTRODUCTION

It is today well known that two important determinants of whole blood viscosity, i.e., red blood cell (RBC) deformability and aggregation, must be carefully regulated to avoid an unusual hemodynamical behavior in the circulatory system. Many diseases, such as cardiovascular ones,[1] diabetes,[2] inherited sickle-cell disease,[3] and malaria,[4] can lead to a hardening of RBCs and more intense aggregation to occur, leading to an increase in blood viscosity compared to healthy individuals. Given that diseases of the circulatory system are (in 2017) the deadliest diseases in the EU,[5] and possibly globally, it is very important to be able to perform *in silico* simulations in order to accurately describe the complex rheological behavior of blood in our circulatory system. Given the advances made in performing flow simulations of blood nowadays,[6] such a task is certainly not daunting. This would allow for an early detection of circulatory diseases and for the more effective development of cardiovascular devices, such as heart valves or stents.[1]

Our circulatory system is primarily comprised of two interconnected subsystems with varied functionality: macrocirculation, i.e., blood flows through large elastic arteries and transports oxygen and metabolites, and microcirculation, i.e., nutrient-rich blood flows from the left ventricle to the small arteries such as prearterioles, arterioles, and capillaries, which help in distributing blood to the organs and body tissues.[7] Normal blood is a highly complicated, viscoelastic and thixotropic, non-Newtonian fluid consisting of blood cells suspending in plasma (a Newtonian fluid, with a typical viscosity of about 1.2 mPa s at 37 °C[8]) composed mostly of water and proteins. In addition to RBCs, blood cells include white blood cells and platelets, with RBCs consisting the vast majority (by ~98%); thus, the

rheology of blood is primarily determined by the rheological behavior of RBCs.[1,9] Under physiological conditions, RBCs constitute 47% in men and 42% in women of the blood volume, the so-called hematocrit (Ht).[8] RBCs are shaped as biconcave disks with a disk diameter equal to 6 μm–9 μm, whereas its thickness at the thickest point is about 1.84 μm–2.84 μm and its minimum thickness in the center is about 0.81 μm–1.44 μm. The typical volume of a RBC is equal to 90 μm^3.[9] RBCs are very deformable since they are composed of a thin elastic membrane (lipid bilayer) enclosing the cytoplasm (a hemoglobin solution),[9] which has a higher viscosity, equal to about 3 mPa s–10 mPa s,[10] than that of the surrounding blood plasma. Thus, the ratio of the internal (cytoplasm) and external (plasma) viscosities, λ_η, is between 2.5 and 8.3. Under physiological conditions, it is today well known that due to the presence of plasma proteins, primarily fibrinogen, RBCs under low flow rates or at stasis spontaneously stick to each other, forming stack-of-coins formations termed rouleaux[11] that considerably affect blood viscosity, whereas at even lower flow rates they form a three-dimensional network,[12] leading to the exhibition of a yield stress.[13]

The viscosity of normal human blood, i.e., blood with a hematocrit value of about 42%–47%, at steady-state exhibits three distinct regions: a lower Newtonian region (reaching the low-rate viscosity, η_0), an upper Newtonian region (reaching the high-rate viscosity, η_∞), and the intermediate region where the viscosity is decreasing with increasing shear rate, i.e., the blood is shear thinning.[9,14,15] This non-Newtonian behavior of blood is attributed to the aggregation of RBCs at lower shear rates, while as the shear rate increases, the RBC deformability becomes more and more influential and eventually predominant after about 10 s^{-1}.[16,17] Both factors, aggregability and deformability, affect blood rheology under different conditions. In large arterial blood vessels (with a diameter larger than 1 mm), large shear rates occur leading to the destruction of any aggregates, and thus, the deformation of single RBCs is the only factor affecting blood viscosity.[9] Deformation also plays a predominant role in capillaries, i.e., vessels that are smaller than the RBCs at rest, where the RBCs must deform in order to enter.[13] On the other hand, blood is noted to be non-Newtonian due to RBC aggregation in regions where low shear exists, such as near bifurcations, anastomoses, stenoses, and aneurysms,[9] but also in the neural network.[18] Finally, when one is interested in the steady-state rheological behavior of blood, we also need to consider that blood is noted to be viscoelastic, first reported by Thurston[19] who showed that the elastic properties of whole human blood decrease with increasing shear rate. He later conducted oscillatory experiments of whole blood to determine their viscoelastic behavior and showed that it diminishes at higher shear rates and noted evidence that suggests that blood exhibits a very broad spectrum of relaxation times.[20]

In addition to steady-state rheology, we also need to examine the time-dependent rheology of whole blood. This is particularly important as blood in circulation experiences rapid and cyclic changes from low- to high-shear flow conditions during the cardiac cycle.[1] Besides, thixotropy is inherently linked with time-dependent changes. Thixotropy is defined, according to IUPAC, as the continuous decrease of the viscosity with time when flow is applied to a sample that has been previously at rest and the subsequent recovery of viscosity in time when the flow is discontinued.[21] For example, when suddenly stepping up or down the shear rate, the viscosity transients obtained reflect the changes in the microstructure. In particular, the growth of the viscosity after a sudden decrease in the shear rate is an indication of thixotropy and could be employed to test the applicability of thixotropic models.[21] It is, thus, apparent that if we aspire to accurately simulate the, both steady-state and time-dependent, rheological behavior of whole blood in both macrocirculation and microcirculation, a constitutive model addressing aggregability, deformability, and thixotropy is certainly needed.

From a modeling standpoint, a plethora of constitutive models have been developed aiming to address the peculiar rheological behavior of blood. As mentioned above, under certain conditions, e.g., in large arterial blood vessels, blood can be considered as a Newtonian fluid. In this case, a considerable amount of work has been devoted to unveiling the dependency of the viscosity on the hematocrit, the plasma viscosity, and the maximum packing fraction.[9] When shear-thinning needs to be considered, several generalized, steady-state models can be used such as the Cross, Carreau, Carreau-Yasuda, Quemada, Herschel–Bulkley (see, e.g., Valant *et al.*[15] where the regularized version of the Herschel–Bulkley constitutive equation is employed as proposed by Papanastasiou[22]), and Casson models,[9] with the last three allowing for the prediction of a yield stress. More recently, some of these have been used as the basis to provide a more elaborate dependency on various important parameters, such as the generalization of the Casson model by Apostolidis and Beris[23] who considered both the viscosity and yield stress of blood to depend on the hematocrit, the temperature, and the fibrinogen concentration. Viscoelasticity has also been considered via the use of the Oldroyd-B and the Yeleswarapu models[9] as well as the generalized Oldroyd-B and Maxwell constitutive models developed by Anand and Rajagopal[24–26] on thermodynamic principles. More recently, other viscoelastic models that are routinely employed to address the viscoelasticity of polymeric materials have also been employed to address the viscoelasticity of blood, such as the Giesekus and Phan-Thien Tanner ones.[27,28] However, perhaps the most sophisticated model is the generalized Maxwell-type model of Owens,[29] who considered blood as an ensemble of rouleaux, each rouleau modeled as an elastic dumbbell. He accounted for the rouleaux aggregation and disaggregation by employing ideas from the temporary polymer network theory, whereas the kinetic rates needed were obtained by simply fitting experimental data. We have recently[30] proposed a modified version of the Owens model by using the generalized bracket formalism of non-equilibrium thermodynamics (NET),[31] which has the appealing advantage of deriving the aggregation/disaggregation kinetic rates in a self-consistent manner, thus avoiding the need to resort to phenomenological expressions altogether. We treated rouleaux formation and dissociation as a set of two-way (reversible) reactions, each characterized by a forward and a reverse rate.[30]

All the above models, however, fail to address the thixotropic nature of blood under physiological conditions. To do this, we need to identify the evolving blood microstructure that can depend on the shear history.[21] The most common approach is using structural kinetic models, wherein the internal structure is mathematically characterized by a scalar structural variable that expresses the instantaneous degree of structure: in a fully structured state, i.e., a complete network that deforms elastically, it is equal to unity, while in a completely broken state it vanishes.[21] Thus, the most appropriate

constitutive models that must be employed in order to address the complicated rheological behavior of normal blood are the thixo-elasto-viscoplastic ones.[32–36] However, in all these models, the structural variables employed were not directly related to the microstructural characteristics of blood. For example, Stephanou and Georgiou[33] had considered a contravariant conformation tensor to characterize the deformation of the underlying structure, whereas Tsimouri *et al.*,[30] following Owens,[29] modeled each rouleau as an elastic dumbbell characterized by a contravariant conformation tensor. Furthermore, all aforementioned models characterize the deformation of single RBCs using a spring, whereas it is more natural, as described above, to model single RBCs as volume-preserving droplets (when incompressibility applies). As such, and despite the evidence highlighting the significance of accurately predicting the deformability of RBCs, constitutive models properly accounting for the deformability of RBCs are absent in the literature.

To remedy the latter shortcoming, we have recently proposed a detailed model wherein RBCs are described by a conformation tensor constrained to have a constant determinant, which has been used in the past to model emulsions.[37–41] However, that approach can only address non-aggregating blood, which severely limits its applicability. As mentioned in the Conclusions of Ref. 37, to account for the aggregation of RBCs occurring in normal blood, we may follow one of two possible methodologies: The first includes allowing the RBCs to aggregate by considering a set of two-way aggregation/disaggregation reactions, following our own recent work.[30] Then, we may identify the structural variable for single RBCs to be the determinant-conserving conformation tensor $\mathbf{S}$ introduced in Ref. 37 instead of the unconstrained conformation tensor $\mathbf{C}^{(1)}$ introduced in Ref. 30. Despite the fact that this methodology would allow us to address the deformability of RBCs and to properly address the shear-rate dependency of the rouleaux size distribution function without phenomenological modeling, it would not allow for the prediction of a yield stress. On the other hand, the second methodology, which is the one to be followed in this work, follows closely Stephanou and Georgiou[33] and dictates the use of one additional scalar structural variable to properly characterize the network formed by RBCs under small shear rates. However, contrary to the work of Stephanou and Georgiou,[33] we should herein consider a determinant-constrained conformation tensor $\mathbf{S}$.

In our present work, as in our previous works,[30,33,37] we employ the generalized bracket[31] formalism of NET to derive the new hemorheological model so as to properly address three key issues: (a) the selection of the proper state variables, (b) the construction of both the Poisson and dissipation brackets, and (c) the specification of the system's Hamiltonian. The use of a NET formalism guarantees that the constitutive model will be, by construction, consistent with the laws of thermodynamics.[31,43–45] Up to date, NET has been employed to address several micro-structured systems, such as, but not limited to, liquid crystals,[46,47] immiscible complex fluids,[38–41] blood,[30,37] polymer melts and solutions,[31,43–45,48–50] polymer nanocomposites,[51–54] micellar systems,[55,56] drilling fluids,[57] and thixotropic fluids.[33]

The rest of the paper is organized as follows: in Sec. II, we present the derivation of the new constitutive model by extending the one of Stephanou and Tsimouri[37] and provide the governing equations in a non-dimensional form along with a detailed description of the model parameters. We then proceed with Sec. III where the parameterization of the new model is presented, followed by a comparison against the experimental measurements of Sousa *et al.*[58] and Bureau *et al.*[59] in Sec. IV. Our paper concludes with Sec. V where we summarize our work and provide a brief discussion of future plans.

II. DERIVATION OF THE NEW MODEL

A. The vector of state variables

We consider a homogeneous, isothermal, and incompressible flow, meaning that both the total mass density, ρ, and the entropy density (or temperature) are excluded from the vector of state variables. Following previous works,[37–41] in order to describe the rheology and microstructure of RBC suspensions, we consider RBCs as emulsions with droplet morphology by using a constrained contravariant second-rank tensor, $\tilde{\mathbf{S}}$, such that $\det\tilde{\mathbf{S}}$ is equal to the volume of a RBC. We also define the dimensionless tensor $\mathbf{S} = \tilde{\mathbf{S}}/\left(\det\tilde{\mathbf{S}}\right)^{1/3}$ so that $\det\mathbf{S} = 1$. The square root of the eigenvalues of the volume-preserving tensor $\mathbf{S}$ corresponds to the dimensionless semi-axes of the RBCs, with the semi-axes having been made dimensionless using the equilibrium RBC equivalent radius.[37] The simplest possible approximation to the shape of RBCs is spheroidal (i.e., ellipsoids of which the lengths of two axes are the same) so that at equilibrium the tensor $\tilde{\mathbf{S}}$ is equal to $\mathrm{diag}\left[a^2, a^2, c^2\right]$, where a and c are the principal semi-axes of the RBC (see Fig. 1 of Ref. 37), whose determinant is $\det\tilde{\mathbf{S}} = \det\tilde{\mathbf{S}}_{eq} = a^4c^2 = \left[3V_{\mathrm{RBC}}/(4\pi)\right]^2$; since the volume of a spheroid is $V_{\mathrm{RBC}} = (4\pi/3)a^2c$, then $\mathbf{S}_{eq} = \tilde{\mathbf{S}}_{eq}/\left(\det\tilde{\mathbf{S}}_{eq}\right)^{1/3} = \mathrm{diag}\left[(a/c)^{2/3}, (a/c)^{2/3}, (c/a)^{4/3}\right]$. Considering the typical values $2a = 7.5\ \mu$m and $V_{\mathrm{RBC}} = 90\ \mu\mathrm{m}^3$, we must consider $c = 3.06\ \mu$m.[37] Next, to account for the tendency of RBCs to aggregate in normal blood, we here employ one additional scalar structural variable, λ, to properly characterize the network formed by RBCs under sufficiently small shear rates. When the network is fully formed, then $\lambda = 1$, while in a completely broken state, i.e., when only single RBCs remain, λ vanishes.[21,33] Finally, we consider the momentum density $\mathbf{M}$ as the hydrodynamic variable. Overall, the vector $\mathbf{x}$ of state variables is expressed as $\mathbf{x} = \{\mathbf{M}, \mathbf{S}, \lambda\}$.

B. The Hamiltonian of the system

The mechanical part of the system's Hamiltonian is given by[31]

$$H_m = K_{en}(\mathbf{x}) + A(\mathbf{x}), \tag{1}$$

where

$$K_{en}(\mathbf{x}) = \int \frac{\mathbf{M}^2}{2\rho} dV. \tag{2}$$

The first term on the right-hand side of Eq. (1) represents the kinetic energy of the system, $K_{en}(\mathbf{x})$, given by Eq. (2), whereas $A(\mathbf{x})$ represents the system's Helmholtz free energy, for which we consider here the following form:[33,37]

$$A(\mathbf{C}, \lambda) = Ht\Gamma \int I_2^C dV + Ht\Gamma \int (\lambda \ln\lambda - \lambda + 1) dV, \tag{3a}$$

where I_2^C is the second invariant of the tensor $\mathbf{C}$ such that $\mathbf{S} = \mathbf{C}\cdot\mathbf{S}_{eq} \Rightarrow \mathbf{C} = \mathbf{S}\cdot\mathbf{S}_{eq}^{-1}$, i.e., $\mathbf{C}_{eq} = \mathbf{I}$ (see Ref. 37), Ht is the hematocrit, and $\Gamma = E_{eq}\gamma/V_{RBC} = \frac{3}{2}(\gamma/c)\left[1+\left(e^{-1}-e\right)\tanh^{-1}e\right]$ is the surface energy density, where $E_{eq} = 2\pi a^2\left[1+\left(e^{-1}-e\right)\tanh^{-1}e\right]$ is the spheroid surface area with $e^2 = 1-(c/a)^2$, and γ is the surface tension. The first integral in Eq. (3a) is the simplest possible expression for the interfacial energy of the RBC.[37] Note that, in general, this term should be a function of only the first two invariants of $\mathbf{C}$ (since the third, the determinant, is constant), and more general expressions could be used, such as the one proposed by Mwasame *et al.*[41] or the one proposed by Skalak *et al.*[60] to specifically address the deformation of the RBC membrane. Despite the availability of such more elaborate free energy expressions, we choose to consider in our present work the simplest possible expression. The second integral indicates the ideal entropy of mixing for segments that are not associated with the network with an extra term added to ensure that the mixing free energy maximizes under no flow conditions, i.e., when $\lambda = 1$.[33] Following Mwasame *et al.*,[41] the surface energy density for spherical at equilibrium droplets is given as $\Gamma = 3\gamma/R$, where R is the radius of the droplet. Considering that the value of the surface energy density is in general applicable only for dilute RBC suspensions, we here consider[37]

$$\gamma = f_0\gamma_0 \Rightarrow \Gamma = f_0\Gamma_0, \quad \Gamma_0 = \frac{3\gamma_0}{R}, \tag{3b}$$

where γ_0 is the surface tension in infinite dilution. Although Stephanou and Tsimouri[37] had considered f_0 to be a function of various parameters to match the model prediction of the zero-rate shear viscosity with the expected experimental result, here we choose to consider it as an adjustable parameter since such a matching cannot take place as the zero-rate shear viscosity of normal blood is difficult to be measured.

C. The Poisson and dissipation brackets

Following Edwards *et al.*[61] and Beris and Edwards,[31] the Volterra derivative of the constrained tensor $\mathbf{S}$ related to the unconstrained tensor $\mathbf{B}$ via $\mathbf{S} = \mathbf{B}/(\det\mathbf{B})^{1/3}$ is given as

$$\frac{\delta}{\delta B_{\alpha\beta}} = \frac{1}{(\det\mathbf{B})^{1/3}}\left(\delta_{\alpha\mu}\delta_{\beta\nu} - \frac{1}{3}S_{\mu\nu}S^{-1}_{\alpha\beta}\right)\frac{\delta}{\delta S_{\mu\nu}}. \tag{4}$$

For a system described by an unconstrained conformation tensor $\mathbf{B}$, the expression for the Poisson bracket is well known (see, e.g., Refs. 31 and 43):

$$\begin{aligned}\{F,G\}_B = &-\int\left[\frac{\delta F}{\delta M_\gamma}\nabla_\beta\left(M_\gamma\frac{\delta G}{\delta M_\beta}\right) - \frac{\delta G}{\delta M_\gamma}\nabla_\beta\left(M_\gamma\frac{\delta F}{\delta M_\beta}\right)\right]dV\\ &-\int\left[\frac{\delta F}{\delta B_{\alpha\beta}}\nabla_\gamma\left(B_{\alpha\beta}\frac{\delta G}{\delta M_\gamma}\right) - \frac{\delta G}{\delta B_{\alpha\beta}}\nabla_\gamma\left(B_{\alpha\beta}\frac{\delta F}{\delta M_\gamma}\right)\right]dV\\ &-\int B_{\alpha\gamma}\left[\frac{\delta G}{\delta B_{\alpha\beta}}\nabla_\gamma\left(\frac{\delta F}{\delta M_\beta}\right) - \frac{\delta F}{\delta B_{\alpha\beta}}\nabla_\gamma\left(\frac{\delta G}{\delta M_\beta}\right)\right]dV\\ &-\int B_{\beta\gamma}\left[\frac{\delta G}{\delta B_{\alpha\beta}}\nabla_\gamma\left(\frac{\delta F}{\delta M_\alpha}\right) - \frac{\delta F}{\delta B_{\alpha\beta}}\nabla_\gamma\left(\frac{\delta G}{\delta M_\alpha}\right)\right]dV.\end{aligned} \tag{5}$$

Note that here, and throughout this work, Einstein's summation convention for repeated Greek indices is employed. Then, by using Eq. (4) in the Poisson bracket, we get[31,37–41]

$$\begin{aligned}\{F,G\}_S = &-\int\left[\frac{\delta F}{\delta M_\gamma}\nabla_\beta\left(M_\gamma\frac{\delta G}{\delta M_\beta}\right) - \frac{\delta G}{\delta M_\gamma}\nabla_\beta\left(M_\gamma\frac{\delta F}{\delta M_\beta}\right)\right]dV\\ &-\int\left[\frac{\delta F}{\delta S_{\alpha\beta}}\frac{\delta G}{\delta M_\gamma}\nabla_\gamma S_{\alpha\beta} - \frac{\delta G}{\delta S_{\alpha\beta}}\frac{\delta F}{\delta M_\gamma}\nabla_\gamma S_{\alpha\beta}\right]dV\\ &-\int S_{\alpha\gamma}\left[\frac{\delta G}{\delta S_{\alpha\beta}}\nabla_\gamma\left(\frac{\delta F}{\delta M_\beta}\right) - \frac{\delta F}{\delta S_{\alpha\beta}}\nabla_\gamma\left(\frac{\delta G}{\delta M_\beta}\right)\right]dV\\ &-\int S_{\beta\gamma}\left[\frac{\delta G}{\delta S_{\alpha\beta}}\nabla_\gamma\left(\frac{\delta F}{\delta M_\alpha}\right) - \frac{\delta F}{\delta S_{\alpha\beta}}\nabla_\gamma\left(\frac{\delta G}{\delta M_\alpha}\right)\right]dV\\ &+\frac{1}{3}\int S_{\alpha\beta}S^{-1}_{\rho\eta}\left(\frac{\delta G}{\delta S_{\alpha\beta}}\frac{\delta F}{\delta M_\gamma} - \frac{\delta F}{\delta S_{\alpha\beta}}\frac{\delta G}{\delta M_\gamma}\right)\nabla_\gamma S_{\rho\eta}dV\\ &+\frac{2}{3}\int S_{\alpha\beta}\left[\frac{\delta G}{\delta S_{\alpha\beta}}\nabla_\gamma\left(\frac{\delta F}{\delta M_\gamma}\right) - \frac{\delta F}{\delta S_{\alpha\beta}}\nabla_\gamma\left(\frac{\delta G}{\delta M_\gamma}\right)\right]dV.\end{aligned} \tag{6a}$$

Furthermore, we consider the following expression for the Poisson bracket associated with the scalar structural variable λ:[33,43]

$$\begin{aligned}\{F,G\}_\lambda = &-\int\left[\frac{\delta F}{\delta\lambda}\nabla_\gamma\left(\lambda\frac{\delta G}{\delta M_\gamma}\right) - \frac{\delta G}{\delta\lambda}\nabla_\gamma\left(\lambda\frac{\delta F}{\delta M_\gamma}\right)\right]dV\\ &-\int g_{\gamma\alpha}\left[\frac{\delta G}{\delta\lambda}\nabla_\gamma\left(\frac{\delta F}{\delta M_\alpha}\right) - \frac{\delta F}{\delta\lambda}\nabla_\gamma\left(\frac{\delta G}{\delta M_\alpha}\right)\right]dV.\end{aligned} \tag{6b}$$

The last integral in Eq. (6b) introduces a general coupling between the scalar structural variable and the velocity gradient through the tensor $\mathbf{g}$.[43] The Poisson bracket of the system is then simply $\{F,G\} = \{F,G\}_S + \{F,G\}_\lambda$.

Next, for the dissipative bracket, we again choose a form that is frequently employed,[31,33,37,43]

$$\begin{aligned}[F,G]_{nec} = &-\int\frac{\delta F}{\delta B_{\alpha\beta}}\bar{\Lambda}_{\alpha\beta\gamma\varepsilon}\frac{\delta G}{\delta B_{\gamma\varepsilon}}dV - \int\frac{\delta F}{\delta\lambda}\Lambda^\lambda\frac{\delta G}{\delta\lambda}dV\\ &+\int\bar{L}_{\alpha\beta\gamma\varepsilon}\left[\frac{\delta F}{\delta B_{\gamma\varepsilon}}\nabla_\alpha\left(\frac{\delta G}{\delta M_\beta}\right) - \frac{\delta G}{\delta B_{\gamma\varepsilon}}\nabla_\alpha\left(\frac{\delta F}{\delta M_\beta}\right)\right]\\ &-\int\nabla_\alpha\left(\frac{\delta F}{\delta M_\beta}\right)Q_{\alpha\beta\gamma\varepsilon}\nabla_\gamma\left(\frac{\delta G}{\delta M_\varepsilon}\right)dV.\end{aligned} \tag{7}$$

The first two integrals on the right-hand side of Eq. (7) account for relaxation effects for an unconstraint conformation tensor $\mathbf{B}$, proportional to a fourth-rank relaxation tensor $\bar{\mathbf{\Lambda}}$, and the scalar structural variable λ. The third integral will allow us to introduce RBC tumbling by considering non-affine deformation,[37] whereas the last integral, proportional to the fourth-rank tensor $Q_{\alpha\beta\gamma\varepsilon}$, aims to add an additional Newtonian-like rheological contribution to the stress tensor. Note that the subscript "nec," meaning "no entropy production correction," is added to the dissipation bracket to indicate that this dissipation bracket is without terms involving Volterra derivatives with respect to the entropy density.[31] These terms are unimportant when one considers (as we do here) isothermal systems. Finally, using Eq. (4), the corresponding terms of the dissipation bracket

related to the determinant-constrained tensor **S** are obtained as

$$[F,G]_{nec} = -\int\left(\delta_{\alpha\mu}\delta_{\beta\nu} - \frac{1}{3}S_{\alpha\beta}S^{-1}_{\mu\nu}\right)\frac{\delta F}{\delta S_{\alpha\beta}}\Lambda_{\mu\nu\gamma\varepsilon}\left(\delta_{\gamma\rho}\delta_{\varepsilon\eta} - \frac{1}{3}S_{\rho\eta}S^{-1}_{\gamma\varepsilon}\right) \times \frac{\delta G}{\delta S_{\rho\eta}}dV - \int\frac{\delta F}{\delta\lambda}\Lambda^{\lambda}\frac{\delta G}{\delta\lambda}dV + \int L_{\alpha\beta\gamma\varepsilon}\left(\delta_{\gamma\mu}\delta_{\varepsilon\nu} - \frac{1}{3}S_{\mu\nu}S^{-1}_{\gamma\varepsilon}\right) \times\left[\frac{\delta F}{\delta S_{\mu\nu}}\nabla_{\alpha}\left(\frac{\delta G}{\delta M_{\beta}}\right) - \frac{\delta G}{\delta S_{\mu\nu}}\nabla_{\alpha}\left(\frac{\delta F}{\delta M_{\beta}}\right)\right] - \int\nabla_{\alpha}\left(\frac{\delta F}{\delta M_{\beta}}\right)Q_{\alpha\beta\gamma\varepsilon}\nabla_{\gamma}\left(\frac{\delta G}{\delta M_{\varepsilon}}\right)dV, \tag{8}$$

where $\Lambda_{\alpha\beta\gamma\varepsilon} = \overline{\Lambda}_{\alpha\beta\gamma\varepsilon}/(\det\mathbf{B})^{2/3}$ and $L_{\alpha\beta\gamma\varepsilon} = \overline{L}_{\alpha\beta\gamma\varepsilon}/(\det\mathbf{B})^{1/3}$.[37] Then,

$$\dot{S}_{\alpha\beta,[1]} = -\left(\Lambda_{\alpha\beta\gamma\varepsilon} - \frac{1}{3}S_{\alpha\beta}S^{-1}_{\mu\nu}\Lambda_{\mu\nu\gamma\varepsilon}\right)\left(\frac{\delta H_m}{\delta S_{\gamma\varepsilon}} - \frac{1}{3}S_{\rho\eta}\frac{\delta H_m}{\delta S_{\rho\eta}}S^{-1}_{\gamma\varepsilon}\right) + \left(\delta_{\alpha\gamma}\delta_{\beta\varepsilon} - \frac{1}{3}S_{\alpha\beta}S^{-1}_{\gamma\varepsilon}\right)L_{\mu\nu\gamma\varepsilon}\nabla_{\mu}\frac{\delta H_m}{\delta M_{\nu}},$$

$$\frac{D\lambda}{Dt} \equiv \frac{\partial\lambda}{\partial t} + u_{\gamma}\nabla_{\gamma}\lambda = -\Lambda^{\lambda}\frac{\delta H_m}{\delta\lambda} + \boldsymbol{\kappa}:\mathbf{g}, \tag{9a}$$

where we have also defined the time derivative,

$$\dot{S}_{\alpha\beta,[1]} \equiv \frac{\partial S_{\alpha\beta}}{\partial t} + u_{\gamma}\nabla_{\gamma}S_{\alpha\beta} - S_{\alpha\gamma}\nabla_{\gamma}u_{\beta} - \nabla_{\gamma}u_{\alpha}S_{\gamma\beta} + \frac{2}{3}S_{\alpha\beta}\nabla_{\gamma}u_{\gamma} + \frac{1}{3}S_{\alpha\beta}S^{-1}_{\rho\eta}u_{\gamma}\nabla_{\gamma}S_{\rho\eta} \tag{9b}$$

and the material time derivative,

$$\frac{D\lambda}{Dt} \equiv \frac{\partial\lambda}{\partial t} + \mathbf{u}\cdot\nabla\lambda. \tag{9c}$$

Also, $\boldsymbol{\kappa} = (\nabla\mathbf{u})^T$ is the transposed velocity gradient tensor. Finally, the stress tensor is given as

$$\sigma_{\alpha\beta} = 2\left(S_{\beta\gamma}\frac{\delta A}{\delta S_{\alpha\gamma}} - \frac{1}{3}\delta_{\alpha\beta}S_{\gamma\varepsilon}\frac{\delta A}{\delta S_{\gamma\varepsilon}}\right) + Q_{\alpha\beta\gamma\varepsilon}\nabla_{\gamma}u_{\varepsilon} + L_{\alpha\beta\gamma\varepsilon}\left(\delta_{\gamma\mu}\delta_{\varepsilon\nu} - \frac{1}{3}S_{\mu\nu}S^{-1}_{\gamma\varepsilon}\right)\frac{\delta A}{\delta S_{\mu\nu}} + g_{\alpha\beta}\frac{\delta A}{\delta\lambda}. \tag{10}$$

In the following, we make the choice $\mathbf{g} = -\lambda\mathbf{C}$ that duly satisfies the requirement that the Poisson bracket fulfills the Jacobi identity (see pp. 113–115 of Ref. 43). We now consider the following choices for the **Q** and **L** tensors:

$$Q_{\alpha\beta\gamma\varepsilon} = \eta_{\infty}(Ht,\lambda_{\eta})\left(\delta_{\alpha\gamma}\delta_{\beta\varepsilon} + \delta_{\alpha\varepsilon}\delta_{\beta\gamma}\right),$$
$$L_{\alpha\beta\gamma\varepsilon} = -\frac{\xi}{2}\left(S_{\alpha\gamma}\delta_{\beta\varepsilon} + S_{\alpha\varepsilon}\delta_{\beta\gamma} + S_{\beta\gamma}\delta_{\alpha\varepsilon} + S_{\beta\varepsilon}\delta_{\alpha\gamma}\right). \tag{11}$$

The first expression includes the infinite-rate viscosity, i.e., the viscosity of blood at large shear rates, which depends on both Ht and λ_η via $\eta_\infty = \eta_s P(Ht,\lambda_\eta)$. In the dilute limit, this should be equal to the expression due to Taylor,[62]

$$P(Ht,\lambda_{\eta}) = 1 + HtT(\lambda_{\eta}), \quad T(\lambda_{\eta}) = \frac{5\lambda_{\eta}+2}{2(\lambda_{\eta}+1)}. \tag{12}$$

However, we are here interested in larger (physiological) values of the hematocrit, and thus, we need to employ a generalized version of this expression. We do this by following Krieger and Dougherty[63] (see also Refs. 8 and 53) by selecting

$$P(Ht,\lambda_{\eta}) = \left(1 - \frac{Ht}{Ht_m}\right)^{-T(\lambda_{\eta})Ht_m}, \tag{13}$$

where Ht_m is the maximum packing hematocrit. Note that this expression as $Ht \to 0$ boils down to Taylor's expression. For random close packing of monosized rigid spherical particles, the maximum packing volume fraction is equal to 0.637; however, for spheroids, such as RBCs, this is expected to be larger. Indeed, Donev *et al.*[64] showed that the maximum packing volume fraction depends on the object's shape: for spheres, they found it to be 0.64, whereas for oblate spheroids (M&M candies), it is 0.68. Motivated from this, they performed computer simulations and noted that the maximum packing volume fraction depends on the aspect ratio for both prolate and oblate spheroids. Since RBCs can be approximated as oblate spheroids with a disk equal to approximately $2a = 6\ \mu$m–$9\ \mu$m and a thickest thickness between $2c = 1.84\ \mu$m and $2.84\ \mu$m, meaning that the aspect ratio is between $c/a \approx 0.2$ and 0.5, their simulation results indicate that the maximum packing volume fraction should be between 0.64 and 0.69. However, we should also consider the fact that RBCs are deformable, which would suggest that Ht_m should be even higher. This is verified by the rheological measurements of Tao and Huang[65] who showed that their measured data are in favor of Eq. (13) with $Ht_m = 0.72$ and $T(\lambda_\eta) = 2.3$ that is reasonably close to the value of ≈2.1667 obtained for the average value of $\lambda_\eta = 5$; for completeness, we mention that the value $T(\lambda_\eta) = 2.3$ is obtained when $\lambda_\eta = 9$ that is close to the upper limit of λ_η. In the following, we will assume that $Ht_m = 0.72$ unless otherwise stated.

The second expression in Eq. (11) is the usual expression proposed by Beris and Edwards,[31] which gives rise to the Gordon–Schowalter or Johnson–Segalman time derivative and has also been employed by Mwasame *et al.*;[41] ξ here is the non-affine or slip parameter. This parameter has been related to chain tumbling (rotation) in polymer melts and concentrated polymer solutions[50] but also to RBC tumbling.[37] Therefore, when a non-vanishing non-affine parameter is employed, the RBCs would at small shear rates deform and, once a critical shear rate is exceeded, tumble at larger shear rates, as noted experimentally. In general, its value should be rather small. As also mentioned by Stephanou and Tsimouri,[37] there are no experimental evidence suggesting the consideration of a non-vanishing value of ξ; however, Mwasame *et al.*[41] have shown that, in the case of spherical emulsions at equilibrium, this parameter must be a specific function of the viscosity ratio λ_η in order for their model to recover the asymptotic constitutive equations of up to first-order capillary number microscopic theories. Although such theoretical evidence is absent in the case of emulsions that are ellipsoidal at equilibrium, as we approximate the simplest equilibrium shape of RBCs, we still consider a non-vanishing non-affine parameter that, however, we shall treat simply as a fitting constant. Finally, for the relaxation tensor $\boldsymbol{\Lambda}$ and for Λ^{λ}, we consider the simplest possible expressions,

$$\Lambda_{\alpha\beta\gamma\varepsilon} = \frac{3(1-\lambda)}{4I_2^C\Gamma Ht\tau_S}\left(S_{\alpha\gamma}S_{eq,\beta\varepsilon} + S_{\alpha\varepsilon}S_{eq,\beta\gamma} + S_{\beta\gamma}S_{eq,\alpha\varepsilon} + S_{\beta\varepsilon}S_{eq,\alpha\gamma}\right),$$
$$\Lambda^{\lambda} = \frac{1}{\Gamma Ht\tau_{\lambda}}, \tag{14}$$

where τ_S is a characteristic relaxation time related to the deformability of the RBC[37] and τ_λ is a characteristic relaxation time related to how easily the RBC network can be reconstructed once destroyed due to the applied stresses. Following Mwasame *et al.*,[41] $\tau_S = \eta_S R/\gamma_0$, where $R = 3V_{RBC}/E_{eq}$ is the equivalent RBC radius at equilibrium.[37]

D. The resulting evolution equations

Following the usual procedure,[31] we obtain the following expressions for the evolution equations for the constrained conformation tensor **S** and the scalar structural variable λ:

$$\dot{S}_{\alpha\beta,[JS]} = -\frac{3(1-\lambda)}{I_2\tau_S}\left[-\left(S_{\alpha\gamma}S^{-1}_{eq,\gamma\zeta}S_{\zeta\beta} - \frac{I_1^C}{3}S_{\alpha\beta}\right) - \frac{2I_2^C}{3}\left(S_{eq,\alpha\beta} - \frac{I_2^C}{3}S_{\alpha\beta}\right)\right],$$
$$\frac{D\lambda}{Dt} = -\frac{1}{\tau_\lambda}\ln\lambda - \lambda\boldsymbol{\kappa}:\mathbf{C}, \tag{15a}$$

where the left-hand side defines the Johnson–Segalman time derivative,

$$\dot{S}_{\alpha\beta,[JS]} \equiv \dot{S}_{\alpha\beta,[1]} + \frac{\xi}{2}\left(\dot{\gamma}_{\alpha\gamma}S_{\gamma\beta} + S_{\alpha\gamma}\dot{\gamma}_{\gamma\beta}\right) - \frac{\xi}{3}S_{\alpha\beta}\mathrm{tr}\dot{\boldsymbol{\gamma}}, \tag{15b}$$

and the expression for the extra stress tensor,

$$\sigma_{\alpha\beta} = \frac{6\eta_s}{\tau_S}Htf_0(1-\xi)\left(I_1^C S_{\alpha\gamma}S^{-1}_{eq,\gamma\beta} - S_{\alpha\gamma}S^{-1}_{eq,\gamma\eta}S_{\eta\zeta}S^{-1}_{eq,\zeta\beta} - \frac{2I_2^C}{3}\delta_{\alpha\beta}\right)$$
$$- \frac{3\eta_s}{\tau_S}Htf_0C_{\alpha\beta}(\lambda\ln\lambda) + \eta_\infty(Ht,\lambda_\eta)\dot{\gamma}_{\alpha\beta}. \tag{16}$$

We select to make the stress tensor dimensionless with η_s/τ_s so that

$$\tilde{\sigma}_{\alpha\beta} = 6Htf_0(1-\xi)\left(I_1^C C_{\alpha\beta} - C_{\alpha\gamma}C_{\gamma\beta} - \frac{2I_2^C}{3}\delta_{\alpha\beta}\right) - 3Htf_0C_{\alpha\beta}(\lambda\ln\lambda)$$
$$+ P(Ht,\lambda_\eta)\tilde{\dot{\gamma}}_{\alpha\beta}, \tag{17}$$

where $\tilde{\dot{\boldsymbol{\gamma}}} = \dot{\boldsymbol{\gamma}}\tau_s$ is the dimensionless rate-of-strain tensor. In the following, we will employ the dimensionless parameter $\varepsilon = \tau_\lambda/\tau_S$. As will be shown, in the limit $\varepsilon \to \infty$, this model boils down to the one presented by Stephanou and Tsimouri[37] for non-aggregating blood. As shown in the Appendix, the new model is thermodynamically admissible. In the following, we consider only homogeneous and rectilinear flows.

III. PREDICTIONS OF THE NEW MODEL

In this section, we present the predictions of the new model in shear flow and how they compare with available experimental data. The results have been obtained by numerically solving the constitutive model [Eqs. (15a) and (15b)] using MATLAB.

A. Steady-state predictions

Figure 1 shows the variation of the relative infinite-rate viscosity, η_∞/η_s, given by Eq. (13), as a function of Ht for different values of the parameters λ_η and Ht_m. When the ratio of the internal and external viscosities, λ_η, increases, the relative viscosity curve shifts to higher values, but as the maximum packing hematocrit is reached this deviation diminishes. It should be noted that even the curve

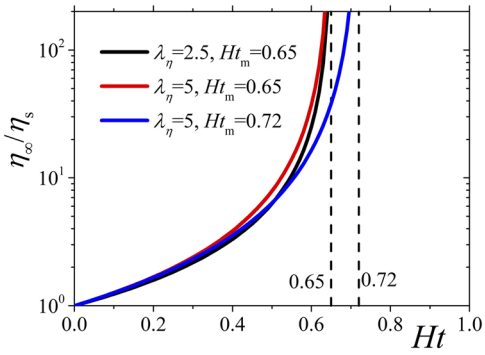

FIG. 1. Theory predictions for the relative infinite-shear-viscosity, η_∞/η_s, as a function of the hematocrit value given by Eq. (13) for various values of the parameters λ_η and Ht_m.

as $Ht \to 0$ shifts to larger Ht values as it follows Taylor's theory: $P(Ht,\lambda_\eta) = 1 + HtT(\lambda_\eta)$, which is accurate up until, approximately, $Ht \approx 0.1$. On the other hand, by increasing the maximum packing hematocrit, the predictions are noted to be the same up until $Ht \approx 0.4$ and shift toward larger Ht values afterward. Overall, this behavior is in accord with available rheological measurements.[65]

In Figs. 2 and 3, we depict the predictions for the dimensionless shear stress [panel (a)] and shear viscosity [panel (b)], while keeping $\lambda_\eta = 2.5$, $Ht = 0.4$, and $Ht_m = 0.72$ (Fig. 2) and $\xi = 0.01$ and $Ht_m = 0.72$ (Fig. 3) fixed. We note in Fig. 2(a) that as the parameter ε decreases, a yield stress, σ_y, is predicted at small shear rates, which is seen to shift to larger values (see the inset). Obviously, in the limit $\varepsilon \to \infty$, the yield stress would vanish, and the model boils down to the one presented by Stephanou and Tsimouri[37] (see also Ref. 33). On the other hand, by increasing the ξ parameter from 0.01 to 0.1 (which is admittedly a relatively large value), a slight shift to smaller values for both the shear stress [Fig. 2(a)] and the shear viscosity [Fig. 2(b)] at small shear rates is noted. Furthermore, by increasing the parameter f_0, the yield shear stress is seen to increase; this is the expected behavior as the exhibition of a yield stress originates from the two first terms of Eq. (16). However, at large shear rates, all curves, irrespective of the values of the parameters ξ and ε, asymptotically reach the Newtonian contribution $P(Ht,\lambda_\eta)$Ca [given by the dotted line in panel (a)]. Overall, the shear stress is what we should expect: a yield shear stress is predicted when a finite, non-vanishing ε parameter is considered [Figs. 2(a) and 3(a)], as expected from rheological measurements of blood at physiological conditions,[14–16,58] the dependence from the ξ parameter seems not to be significant but it would be valuable in numerical simulations in order to consider RBC tumbling (see also Fig. 6), and by increasing the value of the hematocrit, the shear stress curve, and thus the viscosity curve as well, shifts to larger values in agreement with the rheological data of Chien *et al.*,[14] whereas at large enough shear rates, the viscosity eventually reaches a second Newtonian plateau as dictated by numerous rheological data.[14–16,58]

Then, in Figs. 4 and 5, we depict the model predictions for the two dimensionless normal stress differences [panel (a)] and the two dimensionless normal stress coefficients [panel (b)]. We note that in addition to the prediction of a yield first normal stress difference,

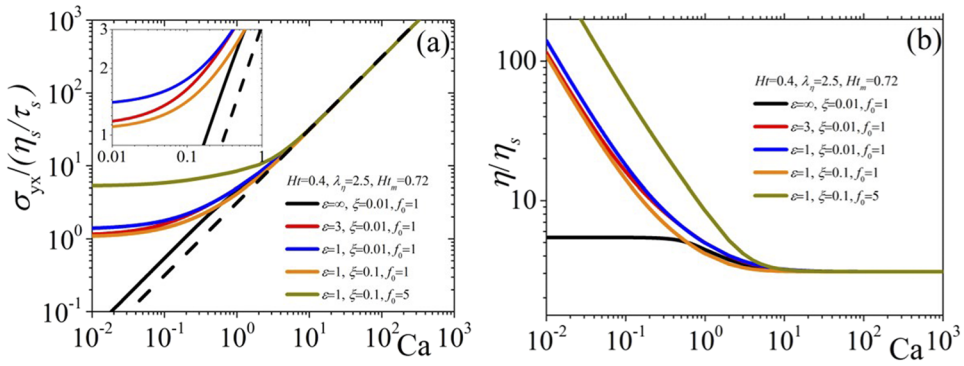

FIG. 2. Model predictions for the dimensionless (a) shear stress and (b) shear viscosity as a function of Ca for various values of the parameters ξ, f_0, and ε, while keeping λ_η = 2.5, Ht = 0.4, and Ht_m = 0.72 fixed. The dotted line in panel (a) depicts the Newtonian contribution of $P(Ht,\lambda_\eta)$Ca.

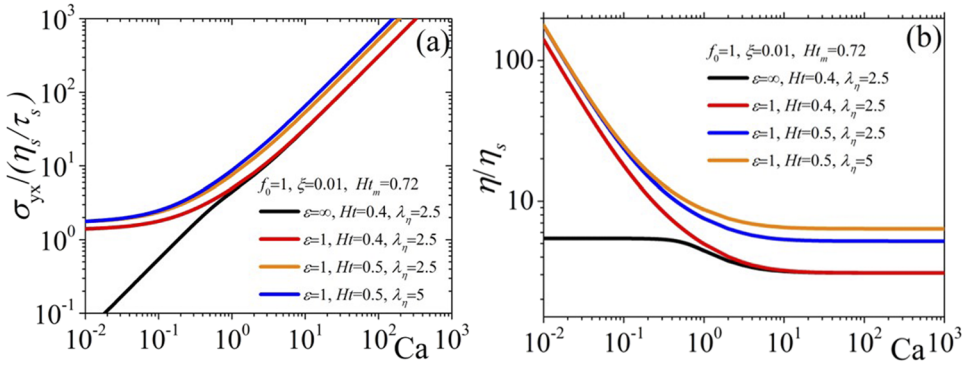

FIG. 3. Model predictions for the dimensionless (a) shear stress and (b) shear viscosity as a function of Ca for various values of the parameters ε, Ht, and λ_η while keeping ξ = 0.01, f_0 = 1, and Ht_m = 0.72 fixed.

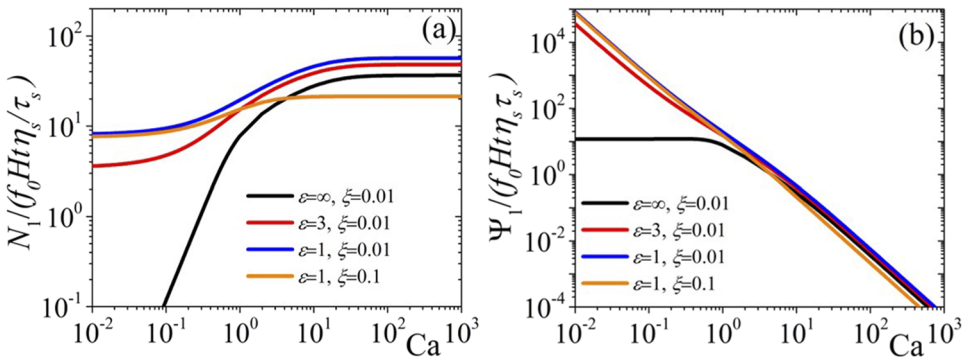

FIG. 4. Model predictions for the dimensionless (a) first normal stress difference and (b) first normal stress coefficient as a function of Ca for various values of the parameters ξ and ε.

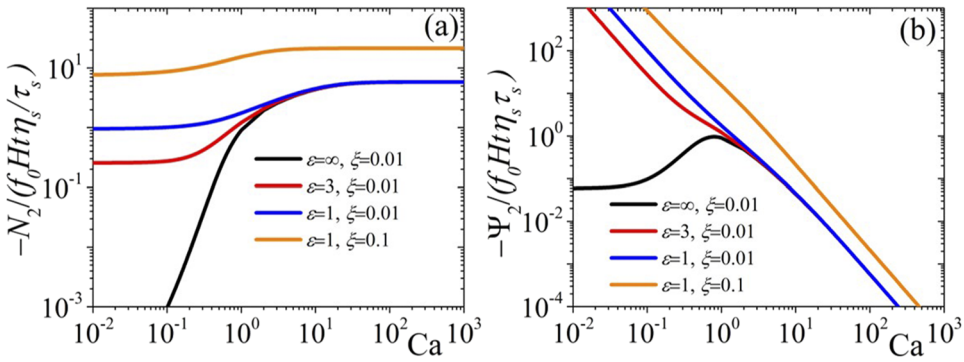

FIG. 5. Model predictions for the negative dimensionless (a) second normal stress difference and (b) second normal stress coefficient as a function of Ca for various values of the parameters ξ and ε.

$N_{1,y}$, when a finite value of the parameter ε is considered, a negative yield second normal stress difference, $N_{2,y}$, is also predicted. This is in disaccord with the model proposed by Stephanou and Georgiou,[33] wherein the second normal stress difference vanishes; this result is a direct consequence of the constant-determinant constraint imposed on the conformation tensor **S** in the present work. We note, as was the case for the shear stress [Figs. 2(a) and 3(a)] and the shear viscosity [Figs. 2(b) and 3(b)], that by decreasing the parameter ε, the yield values are noted to increase (in the limiting case, when $\varepsilon \to \infty$, no yield values are predicted). However, the effect on N_2 is noted to be more significant than that on N_1: when the parameter ξ is increased, the value of $N_{1,y}$ is only slightly affected, whereas N_1 at large shear rates is seen to decrease. On the other hand, the increase of the parameter ξ shifts the whole-N_2 curve upwards. Unfortunately, given the absence of any rheological data concerning the normal stresses of blood, we are not in a position of judging as to whether these predictions are the expected ones. This comment is not restricted only to blood as experimental rheologists have routinely encountered problems in measuring normal stresses in materials known to exhibit a yield shear stress. Only very recently have novel experimental measurements of the yield normal stresses taken place that highlight that not only yield normal stresses are not negligibly small (with $N_1 > 0$ and $N_2 < 0$) but also are as important as the yield shear stress.[66,67] Overall, these recent experimental observations are in accord with the predictions presented above, albeit they do not refer to blood.

B. Inception of simple shear flow

In Fig. 6, we provide the model predictions for the growth of the dimensionless shear viscosity, $(\eta^+ - \eta_\infty)/(f_0 Ht\eta_s)$, wherein we have subtracted the infinite-rate viscosity [panel (a)], and the dimensionless first, $\Psi_1^+/(f_0 Ht\eta_s\tau_s)$ [panel (b)], and negative second, $-\Psi_2^+/(f_0 Ht\eta_s\tau_s)$ [panel (c)], normal stress coefficients as a function of dimensionless time, t/τ_s, for Ca = 1 and 10, and various values of the parameters. At the smaller shear rate (Ca = 1), the first normal stress coefficient is noted to approach its steady-state values monotonically, whereas the shear viscosity and the second normal stress coefficient are noted to go through an overshoot before they reach their steady-state values, which becomes more pronounced by decreasing ε and increasing ξ. Similar conclusions have been noted in our previous model, i.e., when $\varepsilon \to \infty$.[37] On the other hand, at larger shear rates (Ca = 10), we note that all material functions are seen to undergo a dumping behavior, i.e., the appearance of an undershoot following the overshoot, which is more intense in the case of the shear viscosity and the second normal stress coefficient. This behavior intensifies by increasing the value of the non-affine parameter. As noted by Stephanou and Tsimouri,[37] the occurrence of this dumping behavior can be attributed, following similar undershoots appearing in the transient shear viscosity of concentrated polymeric solutions,[50,68,69] to the tumbling behavior of RBCs in simple shear, which has also been observed experimentally (see, e.g., Ref. 24 in Ref. 37). The appearance of such undershoots in the tran-

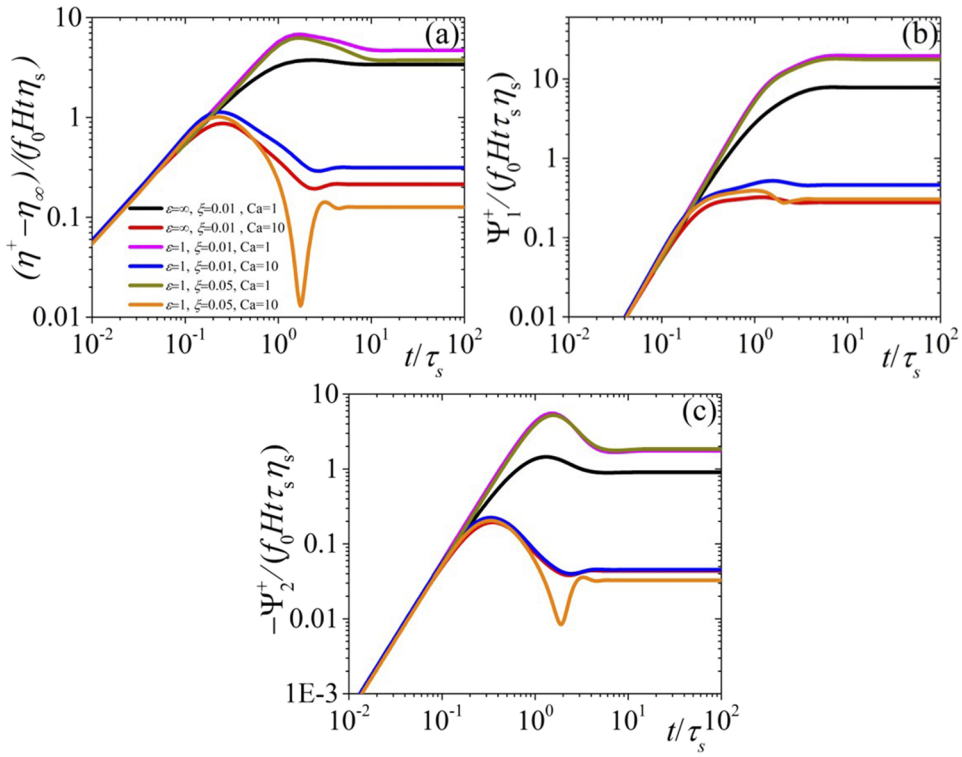

FIG. 6. Growth of the dimensionless (a) shear viscosity, (b) first normal stress coefficient, and (c) second normal stress coefficient upon the inception of simple shear flow at different Ca for various values of the parameters ξ and ε.

sient shear viscosity is in complete accord with recent rheological data.[35]

IV. COMPARISON WITH EXPERIMENTAL DATA

Sousa *et al.*[58] measured the shear stress of a donor's blood for a physiological Ht (41.6%). We consider the plasma viscosity to be equal to η_s = 1.2 mPa s and the average value for the viscosity ratio, i.e., λ_η = 5, meaning that $T(\lambda_\eta) \approx 2.1667$; we further consider Ht_m = 0.72. The remaining parameters (ξ = 0.01, ε = 5, f_0 = 1, and τ_S = 0.06 s) are obtained by simply fitting the model prediction to the experimental data of Sousa *et al.*[58] This comparison is shown in Fig. 7 where we note that the model accurately predicts the experimental data.

Finally, in Fig. 8, we compare the model prediction against the rheological response of normal human blood to a step-change in shear rate experiments (measurements were done at 25 ± 0.5 °C) reported by Bureau *et al.*:[59] at rest, a shear rate equal to 1 s^{-1} is applied, and after 8.5 s, the shear rate is suddenly reduced to zero.

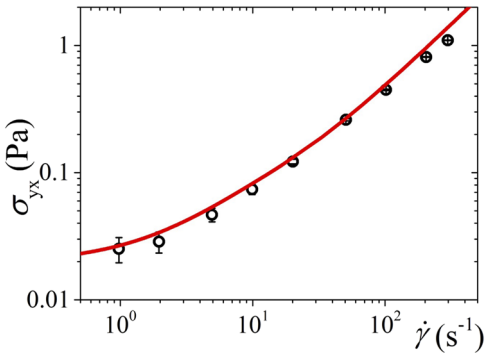

FIG. 7. Comparison of the model predictions (red line) for the shear stress with the experimental rheological data at T = 37 °C (circles) of the blood of Donor A from Sousa *et al.*[58] with Ht = 0.416. Here, Ht_m = 0.72, η_s = 1.2 mPa s, λ_η = 5, ξ = 0.01, ε = 5, f_0 = 1, and τ_S = 0.06 s.

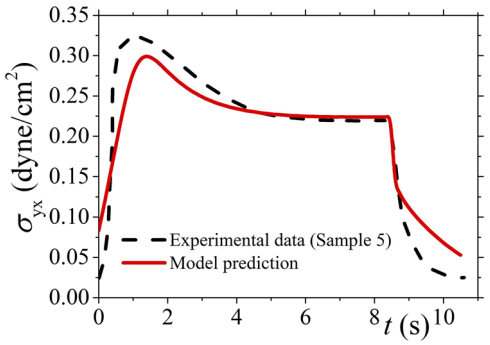

FIG. 8. Comparison of the model predictions (continuous red line) with the experimental step-change in shear rate data (dashed black line) of normal blood sample 5 of Bureau *et al.*[59] at T = 25 °C. Here, Ht = 0.45, Ht_m = 0.72, η_s = 1.8 mPa s, λ_η = 5, ξ = 0.01, ε = 30, f_0 = 4.2, and τ_S = 1 s.

Given that the plasma viscosity at 20 °C is equal to about 2 mPa s[70] and 1.2 mPa s at 37 °C,[6] via linear interpolation, we estimate its value at 25 °C to be about 1.8 mPa s. We will consider a hematocrit equal to 0.45 (as Ref. 59 did not report it), λ_η = 5 meaning that $T(\lambda_\eta) \approx 2.1667$, and Ht_m = 0.72. Then, considering ε = 30, f_0 = 4.2, and τ_S = 1 s, a satisfactory agreement with the experimental data of Bureau *et al.*[59] is noted, although the height of the overshoot is not accurately predicted.

V. CONCLUSIONS

In this work, we have derived a new hemorheological model that addresses self-consistently both the aggregation and deformation of RBCs by extending our previous model wherein we considered only non-aggregating blood.[37] Such an understanding is paramount if we aspire to fully comprehend the rheological behavior of blood in our circulation via the execution of *in silico* simulations. To address the deformability of RBCs, since they are merely droplets with the inner fluid exhibiting a higher viscosity than the outer one, RBCs are considered to be described by a conformation tensor constrained to have a constant determinant following our recent work.[37] Second, we have introduced additional contributions that allow for the prediction of yield values for the shear stress and the two normal stress differences. Since we develop our model in the context of the generalized bracket formalism of NET,[31] the incorporation of the various mechanisms into the constitutive model is done without ambiguities; furthermore, the new model is shown to be thermodynamically admissible (see the Appendix). This is an especially important feature of our work that guarantees the internal consistency of the final dynamical equations. We have shown that the new model is able to accurately predict the rheological response of normal (aggregating) blood: the steady-state shear viscosity as measured by Sousa *et al.*[58] (Fig. 7) and the transient shear viscosity measured in step-change in shear-rate experiments by Bureau *et al.*[59] (Fig. 8).

In addition to the prediction of a yield shear stress, our model predicts yield normal stresses whose physicality cannot be currently judged due to the unavailability of such measurements in the literature. Only recently has experimental evidence emerged highlighting the significance of normal stresses at the yield point,[66,67] leading to the definition of a yield stress tensor.[67] We note the overall qualitative agreement of our model predictions with these recent measurements, but clearly an actual comparison cannot be attempted as these measurements were made for other yield stress materials. Given that, in addition to ours, other theoretical models predict non-vanishing yield normal stresses,[34,71] our work should act as a calling to the experimental rheological community to be more actively interested in measuring yield normal stresses in blood; such measurements could have dire implications to the *in silico* modeling of blood flow.

During the past few decades, drug-carrying, micro- or nano-sized, particles have been used to provide promising and more effective alternative treatments, compared to traditional ones, to fight several diseases. The execution of *in silico* trials (that is, the execution of clinical human trials in computers, i.e., on virtual patients) of such treatments would allow for a faster and more economic design of suitable drug-carrying particles. Given the thermodynamic

nature of our current approach, it can be used in the future to address the transport of drug-carrying particles in our circulation and how this impacts blood rheology. This can be done by introducing one more structural variable, the so-called orientation tensor that describes the average orientation of the particles, following previous works.[51–54] The orientation tensor is constrained to have a constant trace due to the rigidity of the particles considered. Thus, the use of NET can accommodate the consistent incorporation of the new structural variable and its proper coupling with the rest. Such a modification of the present model, i.e., to account for particle advection in our circulation, is expected to be submitted soon for publication.

ACKNOWLEDGMENTS

This work was partially co-funded by the Republic of Cyprus through the Research Promotion Foundation (Project No. POST-DOC/0916/0197).

There are no conflicts to declare.

APPENDIX: THERMODYNAMIC ADMISSIBILITY

Any thermodynamic system must obey the restriction of a non-negative total rate of entropy production. In the case the fluid under study is isothermal and incompressible, the entropy production results from the degradation of the mechanical energy leading to $dH_m/dt = [H_m, H_m] \le 0$.[31] For this to be satisfied in our model, it can be shown that the following condition must hold:

$$-[H_m, H_m] = \int \nabla_\alpha\left(\frac{\delta H_m}{\delta M_\beta}\right) Q_{\alpha\beta\gamma\varepsilon} \nabla_\gamma\left(\frac{\delta H_m}{\delta M_\varepsilon}\right) - \int \Lambda^\lambda \left(\frac{\delta H_m}{\delta \lambda}\right)^2 dV + \int \left(\delta_{\alpha\mu}\delta_{\beta\nu} - \frac{1}{3} S_{\alpha\beta} S^{-1}_{\mu\nu}\right) \frac{\delta H_m}{\delta S_{\alpha\beta}} \times \Lambda_{\mu\nu\gamma\varepsilon}\left(\delta_{\gamma\rho}\delta_{\varepsilon\eta} - \frac{1}{3} S_{\rho\eta} S^{-1}_{\gamma\varepsilon}\right) \frac{\delta H_m}{\delta S_{\rho\eta}} dV \ge 0. \quad \text{(A1)}$$

The first is easily shown to be

$$\int \nabla_\alpha\left(\frac{\delta H_m}{\delta M_\beta}\right) Q_{\alpha\beta\gamma\varepsilon} \nabla_\gamma\left(\frac{\delta H_m}{\delta M_\varepsilon}\right) = \eta_s P(Ht, \lambda_\eta)\dot{\boldsymbol{\gamma}} : \dot{\boldsymbol{\gamma}} \ge 0, \quad \text{(A2)}$$

which holds true for a non-negative solvent viscosity and $P(Ht,\lambda_\eta) \ge 0$; given the use of the particular choice Eq. (13), this condition is satisfied. For the second expression, we only need to make sure that $\Lambda^\lambda \ge 0$, which, as can be seen from Eq. (14), is indeed satisfied given the non-negativity of Γ, Ht, and τ_λ. Finally, for the third expression, we have (see also Ref. 37)

$$\left(\delta_{\alpha\mu}\delta_{\beta\nu} - \frac{1}{3} S_{\alpha\beta} S^{-1}_{\mu\nu}\right) \frac{\delta H_m}{\delta S_{\alpha\beta}} \Lambda_{\mu\nu\gamma\varepsilon}\left(\delta_{\gamma\rho}\delta_{\varepsilon\eta} - \frac{1}{3} S_{\rho\eta} S^{-1}_{\gamma\varepsilon}\right) \frac{\delta H_m}{\delta S_{\rho\eta}} = \frac{3(1-\lambda) Ht \Gamma}{\tau_S}\left\{\mathrm{tr}\mathbf{C}^3 - \mathrm{tr}\mathbf{C}^2 + \frac{2 I_2^C}{3}\left(\frac{2\left(I_2^C\right)^2}{3} - I_1^C\right)\right\}. \quad \text{(A3)}$$

As shown by Stephanou and Tsimouri,[37] using the Caley–Hamilton theorem, one can show that $\mathrm{tr}\mathbf{C}^3 = \left(I_1^C\right)^3 - 3 I_1^C I_2^C + 3$, and noting that $I_1^C \ge 3$ and $I_2^C \ge 3$, then $\mathrm{tr}\mathbf{C}^3 - \mathrm{tr}\mathbf{C}^2 \ge 0$ and $\frac{2}{3}\left(I_2^C\right)^2 - I_1^C \ge 3$, the fact that the parameters Γ, Ht, and τ_R are non-negative and that $0 \le \lambda \le 1$ it is proven that $dH_m/dt = [H_m,H_m] \le 0$. Finally, we need not check whether the conformation tensor is positive-definite since, in the particular application, its determinant is conserved (see also Ref. 37).

DATA AVAILABILITY

The data that support the findings of this study are available from the corresponding author upon reasonable request.

REFERENCES

[1] P. C. Sousa, F. T. Pinho, M. A. Alves, and M. S. N. Oliveira, "A review of hemorheology: Measuring techniques and recent advances," Korea Aust. Rheol. J. **28**, 1–22 (2016).
[2] Y. I. Cho, M. P. Mooney, and D. J. Cho, "Hemorheological disorders in diabetes mellitus," J. Diabetes Sci. Technol. **2**, 1130–1138 (2008).
[3] G. A. Barabino, M. O. Platt, and D. K. Kaul, "Sickle cell biomechanics," Annu. Rev. Biomed. Eng. **12**, 345–367 (2010).
[4] J. P. Shelby, J. White, K. Ganesan, P. K. Rathod, and D. T. Chiu, "A microfluidic model for single-cell capillary obstruction by plasmodium falciparum-infected erythrocytes," Proc. Natl. Acad. Sci. U. S. A. **100**, 14618–14622 (2003).
[5] Eurostat, European Commission, Cardiovascular Diseases Statistics, http://ec.europa.eu/eurostat/statistics-Explained/index.php/Cardiovascular_diseases_statistics (last accessed July 18, 2020).
[6] X. Li, H. Lu, and Z. Peng, "Continuum- and particle-based modeling of human red blood cells," in *Handbook of Materials Modeling*, edited by W. Andreoni and S. Yip (Springer, Cham, 2018).
[7] W. W. Nichols, K. S. Heffernan, and J. A. Chirinos, "Overview of the normal structure and function of the macrocirculation and microcirculation," in *Arterial Disorders*, edited by A. Berbari and G. Mancia (Springer, Cham, 2015).
[8] R. Pal, "Rheology of concentrated suspensions of deformable elastic particles such as human erythrocytes," J. Biomech. **36**, 981–989 (2003).
[9] F. Yilmaz and M. Y. Gundogdu, "A critical review on blood flow in large arteries; relevance to blood rheology, viscosity models, and physiologic conditions," Korea Aust. Rheol. J. **20**, 197–211 (2008).
[10] G. R. Cokelet and H. J. Meiselman, "Rheological comparison of hemoglobin solutions and erythrocyte suspensions," Science **162**, 275–277 (1968).
[11] E. W. Merrill, E. R. Gilliland, G. Cokelet, H. Shin, A. Britten, and R. E. Wells, "Rheology of human blood, near and at zero flow. Effects of temperature and hematocrit level," Biophys. J. **3**, 199–213 (1963).
[12] S. Chen, B. Gavish, S. Zhang, Y. Mahler, and S. Yedgar, "Monitoring of erythrocyte aggregate morphology under flow by computerized image analysis," Biorheology **32**, 487–496 (1995).
[13] O. K. Baskurt and H. J. Meiselman, "Blood rheology and hemodynamics," Semin. Thromb. Hemostasis **29**, 435–450 (2003).
[14] S. Chien, S. Usami, H. M. Taylor, J. L. Lundberg, and M. I. Gregersen, "Effects of hematocrit and plasma proteins on human blood rheology at low shear rates," J. Appl. Physiol. **21**, 81–87 (1966).
[15] A. Z. Valant, L. Ziberna, Y. Papaharilaou, A. Anayiotos, and G. C. Georgiou, "The influence of oxygen concentration on the rheological properties and flow of whole human blood," Rheol. Acta **55**, 921–933 (2016).
[16] O. K. Baskurt, M. R. Hardeman, M. W. Rampling, and H. J. Meiselman, *Handbook of Hemorheology and Hemodynamics* (IOS Press, 2007).
[17] Y. Kim, K. Kim, and Y. Park, "Measurement techniques forRed blood cell deformability: Recent advances," in *Blood Cell: An Overview of Studies in Hematology*, edited by T. E. Moschandreou (IntechOpen, 2012), pp. 167–194.
[18] A. S. Popel and P. C. Johnson, "Microcirculation and hemorheology," Annu. Rev. Fluid Mech. **37**, 43–69 (2005).
[19] G. B. Thurston, "Viscoelasticity of human blood," Biophys. J. **12**, 1205–1217 (1972).
[20] G. B. Thurston, "Frequency and shear rate dependence of viscoelasticity of human blood," Biorheology **10**(3), 375–381 (1973).

[21] J. Mewis and N. J. Wagner, "Thixotropy," Adv. Colloid Interface Sci. **147-148**, 214–227 (2009).
[22] T. C. Papanastasiou, "Flow of materials with yield," J. Rheol. **31**, 385–404 (1987).
[23] A. J. Apostolidis and A. N. Beris, "Modeling of the blood rheology in steady-state shear flows," J. Rheol. **58**, 607–633 (2014).
[24] M. Anand and K. R. Rajagopal, "A shear-thinning viscoelastic fluid model for describing the flow of blood," Int. J. Cardiovasc. Med. Sci. **4**, 59–68 (2004).
[25] M. Anand, J. Kwack, and A. Masud, "A new generalized Oldroyd-B model for blood flow in complex geometries," Int. J. Eng. Sci. **72**, 78–88 (2013).
[26] M. Anand and K. R. Rajagopal, "A short review of advances in the modelling of blood rheology and clot formation," Fluids **2**, 35 (2017).
[27] L. Campo-Deaño, R. P. A. Dullens, D. G. A. L. Aarts, F. T. Pinho, and M. S. N. Oliveira, "Viscoelasticity of blood and viscoelastic blood analogues for use in polydymethylsilox- ane in vitro models of the circulatory system," Biomicrofluidics **7**, 034102 (2013).
[28] A. Shariatkhah, M. Norouzi, and M. R. H. Nobari, "Numerical simulation of blood flow through a capillary using a non-linear viscoelastic model," Clin. Hemorheol. Microcirc. **62**, 109–121 (2016).
[29] R. G. Owens, "A new microstructure-based constitutive model for human blood," J. Non-Newtonian Fluid Mech. **140**, 57–70 (2006).
[30] I. C. Tsimouri, P. S. Stephanou, and V. G. Mavrantzas, "A constitutive rheological model for agglomerating blood derived from nonequilibrium thermodynamics," Phys. Fluids **30**, 030710 (2018).
[31] A. N. Beris and B. J. Edwards, *Thermodynamics of Flowing Systems with Internal Microstructure* (Oxford University Press, New York, 1994).
[32] R. H. Ewoldt and G. H. McKinley, "Mapping thixo-elasto-visco-plastic behavior," Rheol. Acta **56**, 195–210 (2017).
[33] P. S. Stephanou and G. G. Georgiou, "A nonequilibrium thermodynamics perspective of thixotropy," J. Chem. Phys. **149**, 244902 (2018).
[34] M. Clarion, M. Deegan, T. Helton, J. Hudgins, N. Monteferrante, E. Ousley, and M. Armstrong, "Contemporary modeling and analysis of steady state and transient human blood rheology," Rheol. Acta **57**, 141–168 (2018).
[35] J. S. Horner, M. J. Armstrong, N. J. Wagner, and A. N. Beris, "Measurements of human blood viscoelasticity and thixotropy under steady and transient shear and constitutive modeling thereof," J. Rheol. **63**, 799–813 (2019).
[36] S. Varchanis, G. Makrigiorgos, P. Moschopoulos, Y. Dimakopoulos, and J. Tsamopoulos, "Modeling the rheology of thixotropic elasto-visco-plastic materials," J. Rheol. **63**, 609–639 (2019).
[37] P. S. Stephanou and I. Ch. Tsimouri, "A constitutive hemorheological model addressing the deformability of red blood cells in ringer solutions," Soft Matter **16**, 7585–7597 (2020).
[38] M. Dressler and B. J. Edwards, "The influence of matrix viscoelasticity on the rheology of polymer blends," Rheol. Acta **43**, 257–282 (2004).
[39] M. Dressler, B. J. Edwards, and E. J. Windhab, "An examination of droplet deformation and break-up between concentrically rotating cylinders," J. Non-Newtonian Fluid Mech. **152**, 86–100 (2008).
[40] M. Grmela, A. Ammar, F. Chinesta, and G. Maîtrejean, "A mesoscopic rheological model of moderately concentrated colloids," J. Non-Newtonian Fluid Mech. **212**, 1–12 (2014).
[41] P. M. Mwasame, N. J. Wagner, and A. N. Beris, "On the macroscopic modelling of dilute emulsions under flow," J. Fluid Mech. **831**, 433–473 (2017).
[42] P. L. Maffettone and M. Minale, "Equation of change for ellipsoidal drops in viscous flow," J. Non-Newtonian Fluid Mech. **78**, 227–241 (1998).
[43] H. C. Öttinger, *Beyond Equilibrium Thermodynamics* (Wiley-Interscience, NewYork, 2004).
[44] M. Grmela and H. C. Öttinger, "Dynamics and thermodynamics of complex fluids. I. Development of a general formalism," Phys. Rev. E **56**, 6620–6632 (1997).
[45] H. C. Öttinger and M. Grmela, "Dynamics and thermodynamics of complex fluids. II. Illustrations of a general formalism," Phys. Rev. E **56**, 6633–6655 (1997).
[46] B. J. Edwards, A. N. Beris, and M. Grmela, "Generalized constitutive equation for polymeric liquid crystals Part 1. Model formulation using the Hamiltonian (Poisson bracket) formulation," J. Non-Newtonian Fluid Mech. **35**, 51–72 (1990).
[47] B. J. Edwards, A. N. Beris, M. Grmela, and R. G. Larson, "Generalized constitutive equation for polymeric liquid crystals: Part 2. Non-homogeneous systems," J. Non-Newtonian Fluid Mech. **36**, 243–254 (1990).
[48] P. S. Stephanou, I. C. Tsimouri, and V. G. Mavrantzas, "Flow-induced orientation and stretching of entangled polymers in the framework of nonequilibrium thermodynamics," Macromolecules **49**, 3161–3173 (2016).
[49] P. S. Stephanou, C. Baig, and V. G. Mavrantzas, "A generalized differential constitutive equation for polymer melts based on principles of nonequilibrium thermodynamics," J. Rheol. **53**, 309–337 (2009).
[50] P. S. Stephanou, I. Ch. Tsimouri, and V. G. Mavrantzas, "Simple, accurate and user-friendly differential constitutive model for the rheology of entangled polymer melts and solutions from non-equilibrium thermodynamics," Materials **13**, 2867 (2020).
[51] M. Rajabian, C. Dubois, and M. Grmela, "Suspensions of semiflexible fibers in polymeric fluids: Rheology and thermodynamics," Rheol. Acta **44**, 521–535 (2005).
[52] H. Eslami, M. Grmela, and M. Bousmina, "A mesoscopic rheological model of polymer/layered silicate nanocomposites," J. Rheol. **51**, 1189–1222 (2007).
[53] P. S. Stephanou, V. G. Mavrantzas, and G. C. Georgiou, "Continuum model for the phase behavior, microstructure, and rheology of unentangled polymer nanocomposite melts," Macromolecules **47**, 4493–4513 (2014).
[54] P. S. Stephanou, "How the flow affects the phase behaviour and microstructure of polymer nanocomposites," J. Chem. Phys. **142**, 064901 (2015).
[55] N. Germann, L. P. Cook, and A. N. Beris, "Nonequilibrium thermodynamic modeling of the structure and rheology of concentrated wormlike micellar solutions," J. Non-Newtonian Fluid Mech. **196**, 51–57 (2013).
[56] P. S. Stephanou, I. C. Tsimouri, and V. G. Mavrantzas, "Two-species models for the rheology of associative polymer solutions: Derivation from nonequilibrium thermodynamics," J. Rheol. **64**, 1003–1016 (2020).
[57] P. S. Stephanou, "The rheology of drilling fluids from a non-equilibrium thermodynamics perspective," J. Pet. Sci. Eng. **165**, 1010–1020 (2018).
[58] P. C. Sousa, J. Carneiro, R. Vaz, A. Cerejo, F. T. Pinho, M. A. Alves, and M. S. N. Oliveira, "Shear viscosity and nonlinear behavior of whole blood under large amplitude oscillatory shear," Biorheology **50**, 269–282 (2013).
[59] M. Bureau, J. C. Healy, D. Bourgoin, and M. Joly, "Etude rhéologique en régime transitoire de quelques échantillons de sangs humains artificiellement modifiés," Rheol. Acta **18**, 756–768 (1979).
[60] R. Skalak, A. Tozeren, R. P. Zarda, and S. Chien, "Strain energy function of red blood cell membranes," Biophys. J. **13**, 245–264 (1973).
[61] B. J. Edwards, M. Dressler, M. Grmela, and A. Ait-Kadi, "Rheological models with microstructural constraints," Rheol. Acta **42**, 64–72 (2003).
[62] G. I. Taylor, "The viscosity of a fluid containing small drops of another fluid," Proc. R. Soc. London, Ser. A **138**, 41–48 (1932).
[63] I. M. Krieger and T. J. Dougherty, "A mechanism for non-Newtonian flow in suspensions of rigid spheres," Trans. Soc. Rheol. **3**, 137 (1959).
[64] A. Donev, I. Cisse, D. Sachs, E. A. Variano, F. H. Stillinger, R. Connelly, S. Torquato, and P. M. Chaikin, "Improving the density of jammed disordered packings using ellipsoids," Science **303**, 990–993 (2004).
[65] R. Tao and K. Huang, "Reducing blood viscosity with magnetic fields," Phys. Rev. E **84**, 011905 (2011).
[66] R. L. Thompson, L. U. R. Sica, and P. R. de Souza Mendes, "The yield stress tensor," J. Non-Newtonian Fluid Mech. **261**, 211–219 (2018).
[67] H. de Cagny, M. Fazilati, M. Habibi, M. M. Denn, and D. Bonn, "The yield normal stress," J. Rheol. **63**, 285–290 (2019).
[68] P. S. Stephanou, T. Schweizer, and M. Kröger, "Communication: Appearance of undershoots in start-up shear: Experimental findings captured by tumbling-snake dynamics," J. Chem. Phys. **146**, 161101 (2017).
[69] P. S. Stephanou and M. Kröger, "Non-constant link tension coefficient in the tumbling-snake model subjected to simple shear," J. Chem. Phys. **147**, 174903 (2017).
[70] M. Brust, C. Schaefer, R. Doerr, L. Pan, M. Garcia, P. E. Arratia, and C. Wagner, "Rheology of human blood plasma: Viscoelastic versus Newtonian behavior," Phys. Rev. Lett. **110**, 078305 (2013).
[71] C. J. Dimitriou and G. H. McKinley, "A canonical framework for modeling elasto-viscoplasticity in complex fluids," J. Non-Newtonian Fluid Mech. **265**, 116–132 (2019).